DOI: 10.1002/chem.200801265

The Electronic Structure of Iron Corroles: A Combined Experimental and Quantum Chemical Study

Shengfa Ye,[a] Tell Tuttle,[b] Eckhard Bill,[c] Liliya Simkhovich,[d] Zeev Gross,*[d] Walter Thiel,*[b] and Frank Neese*[a, c]

Abstract: There is a longstanding debate in the literature on the electronic structure of chloroiron corroles, especially for those containing the highly electron-withdrawing *meso*-tris(pentafluorophenyl)corrole (TPFC) ligand. Two alternative electronic structures were proposed for this and the related [FeCl(tdcc)] (TDCC = *meso*-tris(2,6-dichlorophenyl)corrole) complex, namely a high-valent ferryl species chelated by a trianionic corrolato ligand ($[Fe^{IV}(Cor)^{3-}]^{+}$) or an intermediate-spin (IS) ferric ion that is antiferromagnetically coupled to a dianionic π-radical corrole ($[Fe^{III}(Cor)^{\bullet 2-}]^{+}$) yielding an overall triplet ground state. Two series of corrole-based iron complexes ([Fe(L)(Cor)], in which L = F, Cl, Br, I, and Cor = TPFC, TDCC) have been investigated by a combined experimental (Mössbauer spectroscopy) and computational (DFT) approach in order to differentiate between the two possible electronic-structure descriptions. The experimentally calibrated conclusions were reached by a detailed analysis of the Kohn–Sham solutions, which successfully reproduce the experimental structures and spectroscopic parameters: the electronic structures of [Fe(L)(Cor)] (L = F, Cl, Br, I, Cor = TPFC, TDCC) are best formulated as ($[IS\text{-}Fe^{III}(Cor)^{\bullet 2-}]^{+}$), similar to chloroiron corrole complexes containing electron-rich corrole ligands. The antiferromagnetic pathway is composed of singly occupied Fe d_{z^2} and corrole a_{2u}-like π orbitals, with coupling constants that exceed those of analogous porphyrin systems by a factor of 2–3. In the corroles, the combination of lower symmetry, extra negative charge, and smaller cavity size (relative to the porphyrins) leads to exceptionally strong iron–corrole σ bonds. Hence, the Fe $d_{x^2-y^2}$-based molecular orbital is unavailable in the corrole complexes (contrary to the porphyrin case), and the local spin states are $S_{Fe} = 3/2$ in the corroles versus $S_{Fe} = 5/2$ in the porphyrins. The consequences of this qualitative difference are discussed for spin distributions and magnetic properties.

Keywords: corroles · density functional calculations · iron · N ligands · non-innocent ligands

[a] Dr. S. Ye, Prof. Dr. F. Neese
Lehrstuhl für Theoretische Chemie, Universität Bonn
Wegelerstrasse 12, 53115 Bonn (Germany)
Fax: (+49) 228-739064
E-mail: neese@thch.uni-bonn.de

[b] Dr. T. Tuttle, Prof. Dr. W. Thiel
Max-Planck-Institut für Kohlenforschung
Kaiser-Wilhelm-Platz 1, 45470 Mülheim an der Ruhr (Germany)
Fax: (+49) 208-306-2996
E-mail: thiel@mpi-muelheim.mpg.de

[c] Dr. E. Bill, Prof. Dr. F. Neese
Max-Planck-Institut für Bioanorganische Chemie
Stiftstrasse 34–37, 45470 Mülheim an der Ruhr (Germany)

[d] Dr. L. Simkhovich, Prof. Dr. Z. Gross
Schulich Faculty of Chemistry
Technion—Israel Institute of Technology
Haifa 32000 (Israel)
Fax: (+972) 4829-5703
E-mail: chr10zg@tx.technion.ac.il

Supporting information for this article is available on the WWW under http://dx.doi.org/10.1002/chem.200801265.

Introduction

Characterization of reactive intermediates involved in the various processes catalyzed by heme enzymes continues to inspire the research of synthetic analogues, from both the experimental and computational points of view.[1] This may be appreciated by the structures depicted in Scheme 1, representing intensely investigated iron porphyrin complexes, in which the overall oxidation state is higher by one (**1**–**3**) and two (**4**) units relative to the iron(III) resting state of the enzymes. Insight into the metal versus porphyrin oxidation dilemma, arising from similar redox potentials of the metal and the porphyrin ligand, has previously been obtained from the combination of various spectroscopic methods, electrochemistry, X-ray crystallography, and computational methods.[2]

The unpaired electrons in **1a** are all of identical spin, while the spin of the single electron from the porphyrin rad-

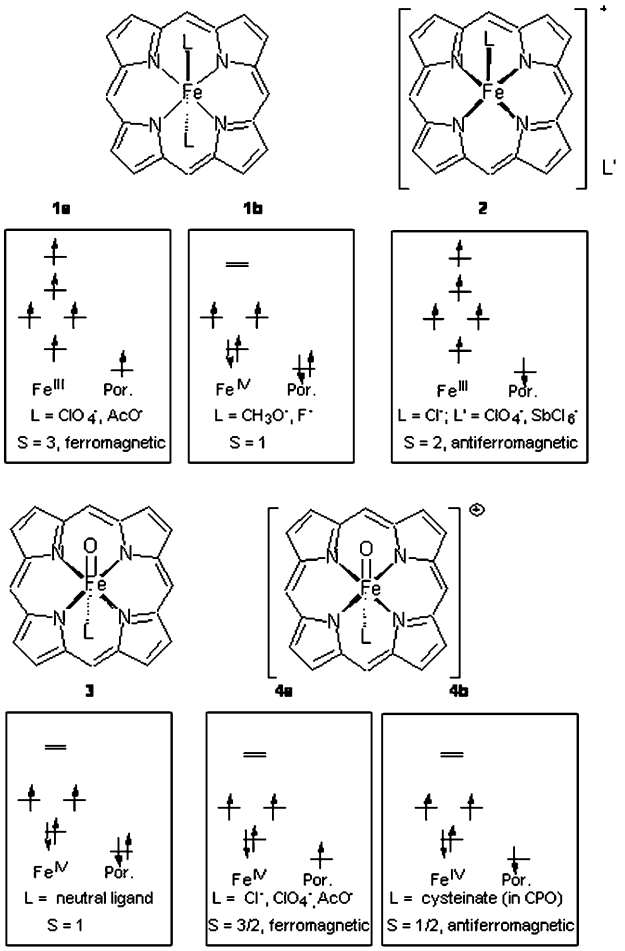

Scheme 1. Electronic configurations of high-valent iron porphyrins: **1**–**3** are one oxidation state above iron(III) porphyrins; **3** represents Compound II; and **4** represents Compound I, which is one oxidation state above **3**.

ical in **2** is opposite to those on iron. These two cases are commonly referred to as ferromagnetic and antiferromagnetic coupling, respectively, adopting the term from bulk magnetic material for describing intramolecular interactions. The influence of the type of axial ligands may be appreciated by the comparison of **1a** with **1b** and of **2** with **3**. Metal rather than porphyrin oxidation as in **1b** and **3** was found to be favored only when the ligands are π-donating (e.g., F^-, CH_3O^-, O^{2-}).[3] Such ligands are known to stabilize high oxidation states of transition metals. A different effect is evident in the doubly oxidized complex **4**, which represents the most important intermediate in catalysis by heme enzymes (Compound I).[4] Possible interactions of the two unpaired electrons in the dπ orbitals with the single porphyrin-based electron were classified as either: strongly ferromagnetic (e.g., in synthetic complexes with L = Cl^-, ClO_4^-, MeOH),[5] exceedingly weak (e.g., in horseradish peroxidase, HRP, L = histidine)[6] and moderately strong antiferromagnetic (e.g., in chloroperoxidase, CPO, L = cysteinate).[1f] In the last case, DFT calculations have provided significant insight into the underlying principles that govern the type and strength of intramolecular interactions between the paramagnetic centers.[7] The last few years have witnessed an enormous increase in the research activities dealing with transition-metal complexes of corroles, the one-carbon-atom-short analogues of porphyrins.[8] The main cause for this renaissance (corroles have been known since 1965) is the simple synthetic access to corroles now available,[9] which in turn triggered their exploration in the many applications that are dominated by porphyrins and related macrocycles. Particularly, metal complexes of tris(pentafluorophenyl)corrole (TPFC) were shown to be promising catalysts,[10] to display unique photophysical properties,[11] and to have significant potential for medical applications.[12]

From the chemical property point of view, iron corroles are quite different from iron porphyrins. This may be exemplified by the oxygenation of iron(III) corroles to binuclear μ-oxoiron(IV) derivatives,[10d] a reaction that takes place with iron(II), but not iron(III), porphyrins. [FeCl(tpfc)] is also the only iron complex that catalyzes the aziridination of olefins by Chloramine-T, a feature that was attributed to a dramatic change in the polarity of the nitrogen atom of the latter upon its coordination to the high valent metal ion.[13] One apparently unresolved issue, however, is the assignment of the electronic states in corrole–metal complexes, the stable oxidation states of which are almost invariably higher by one unit than those of analogous metalloporphyrins.[14,15] A particularly intense debate has centered around complexes with the general formula of [FeCl(Cor)], (**5a**–**8a**; Scheme 2).

Experimental data exists for complexes **6a**–**c**,[16] **7a**–**c**,[17] and **8a**,**b**,[10e,18] including the X-ray structures of **6a**–**c** and **8a**,**b**,[10e,16,18] and computational investigations were reported

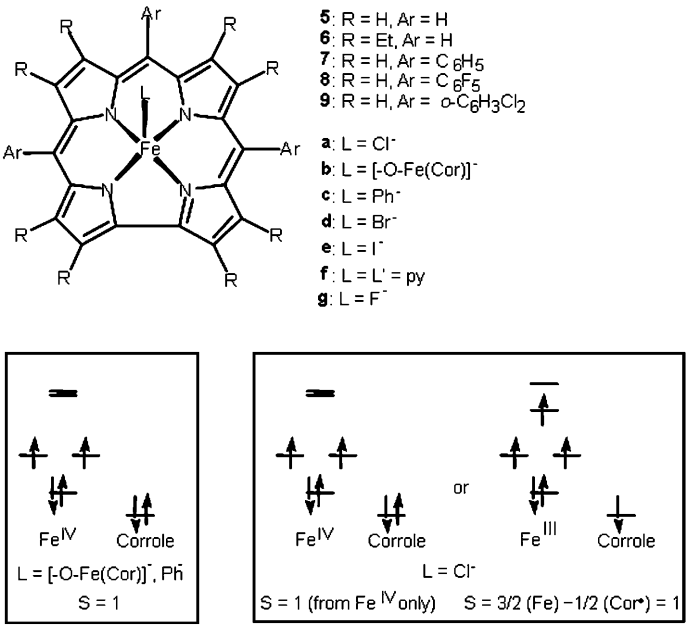

Scheme 2. Formal drawing of five and six-coordinate iron corroles and the two electronic configurations that are consistent with experimental magnetic data.

for **5a–c**,[19,20] **6a**,**c**, and **7a**,**c**.[17] This led to a consensus about the electronic structures of the phenyl- and oxo-ligated iron complexes: a low-spin iron(IV) ($S_{Fe}=1$) that is chelated by the closed-shell corrolato tri-anion and is further charge-balanced by the mono-anionic axial ligand. An identical view was first proposed for the chloro-ligated complex **6a** by Vogel and co-workers,[16] based on the observation of only two unpaired electrons ($S_t=1$, as expected for low-spin iron(IV)) by means of magnetic susceptibility measurements. Gross and co-workers proposed the same description for complex **8a** and provided further support from X-ray crystallography, electrochemistry, and NMR spectroscopy.[10e,18,21] The groups of Ghosh and Walker favored an alternative electronic structure description for complexes **5a–7a**: an intermediate-spin iron(III) ($S_{Fe}=3/2$) that is strongly coupled to an open-shell corrole ($S_{cor}=1/2$) in an antiferromagnetic fashion.[17,19,20]

The strongest experimental support for the iron(III) corrole radical formulation in the case of the chloro-ligated complexes [$Fe^{III}Cl(Me_8Cor)$] and [$Fe^{III}Cl(7,13\text{-}Me_2Et_6Cor)$] comes from the unusually positive ^{1}H NMR chemical shifts (+187 and +174 ppm at 300 K) of their *meso*-hydrogen resonances, analyzed as reflecting large negative spin densities at the *meso*-carbon atoms.[17a,d] This is consistent with DFT calculations on complexes **5a–7a** that revealed large calculated spin densities on the *meso*-carbon atoms for an open-shell corrole ligand.[17d,19] The ^{19}F NMR spectroscopic investigations of **8a** containing a strongly electron-deficient corrole ligand, were not unambiguous in differentiating the two possible electronic configurations,[10e,17b,c] but the very large effects of axial ligands in the [Fe(L)(Cor)] series, in which L=F, Cl, Br, I, and Cor=TPFC, TDCC, on the ^{1}H NMR chemical shifts were analyzed in terms of [$Fe^{IV}(Cor)^{3-}$]. The difference in *meso*-phenyl-H ($\delta_{m\text{-}H}-\delta_{p\text{-}H}$) chemical shifts was proposed as a spectroscopic marker in these molecules.[17b,c,20b] However, this difference shows the same sign and approximately the same magnitude in a quintet chloroiron corrolate complex [$Fe^{III}Cl(OMTPCor)$] (OMTP=2,3,7,8,12,13,17,18-octamethyl-5,10,15-triplhenylcorrolate), in which an intermediate-spin ferric center is *ferromagnetically* coupled to a corrolate radical ligand, and in [$Fe^{III}Cl(7,13\text{-}Me_2Et_6Cor)$] in which these two paramagnetic fragments are antiferromagnetically coupled.[17f]

Potentially, ^{13}C NMR spectroscopy could provide additional strong support for ligand radicals, since it also directly probes the spin populations at the ligand nuclei, in particular for the *meso*-carbon atoms in the substituted corrolate complexes **7a–9a**. However, the signals of *meso*-carbon resonances were too broad to be detected due to unfavorable relaxation rates.[17b] It was also pointed out in the literature that even if such signals could be observed they may not be easily interpreted in terms of spin populations, since "in cases in which the amount of spin density on the macrocycle and axial ligand is found to be too large for simple metal–ligand spin delocalization, a macrocycle radical may be *suspected*".[17e]

The electrochemistry of iron corroles is also distinctively different from that of iron porphyrins.[10e,20] The oxidation potentials of [$Fe^{III}Cl(tpp)$] and [$Ga^{III}Cl(tpp)$] (TPP=*meso*-tetraphenylporphinato) are almost identical ($E_{1/2}=1.13$ and 1.19 V vs. SCE, respectively),[22] consistent with porphyrin oxidation in both cases. On the other hand, [FeCl(tpfc)] displays two redox couples with $E_{1/2}$ values of 0.44 V for [FeCl(tpfc)]/[FeCl(tpfc)]$^-$ and 1.24 V for [FeCl(tpfc)]/[FeCl(tpfc)]$^+$. The second process is consistent with corrole-based oxidation of an iron(IV)-chelated complex, as may be appreciated by the $E_{1/2}$ values of [$Ge^{IV}OH(tpfc)$] and [$Sn^{IV}Cl(tpfc)$] (1.13 and 1.20 V, respectively),[10d] while the first one might be taken as evidence for a metal-based reduction of [FeCl(tpfc)], since it occurs at a lower potential than that of the [Ga(tpfc)]/[Ga(tpfc)]$^+$ redox couple (0.74 V).[10d,11] However, the difference between chloro-coordinated [FeCl(tpfc)] and pyridine-coordinated [Ga(py)(tpfc)] certainly complicates the comparison.

In summary, there is a longstanding controversy concerning the electronic structures of complexes **8a** and the related **9a**.[17b,c,20b] Presumably Mössbauer spectroscopy is the best technique to investigate the question of the most consistent electronic-structure description. The experimental isomer shifts of **5a** and **6a** ($\delta=0.19$–0.21 mm s^{-1}[16,17d]) are, however, at the very high end of what is expected for genuine triplet iron(IV) species. We have therefore decided to re-investigate this issue by a combination of quantum chemistry and Mössbauer spectroscopy, utilizing a variety of halogenoiron corroles rather than just the chloroiron derivatives as in all previous studies. The aim of the current investigation is to provide new theoretical and experimental data in order to reliably determine the complex spin-coupling patterns of these complexes. Specifically, experimental Mössbauer data for two series of corrole-based iron complexes were acquired and DFT calculations were performed. Mössbauer parameters were computed for all structures. Following the reproduction of the experimental geometries and spectroscopic data, the analysis of the obtained Kohn–Sham solutions allows us to draw experimentally calibrated conclusions about the electron and spin distributions in the investigated series of iron corroles and porphyrins.

Results

Mössbauer data and magnetic properties: Mössbauer isomer shifts and quadrupole splittings were measured at 80 K without applied field for the iron complexes of *meso*-tris(pentafluorophenyl)corrole (TPFC) **8a**, **8d**, **8f**, and the iron complexes of *meso*-tris(*o*-dichlorophenyl)corrole (TDCC) **9a**, **9d–f** in the solid state. The results are summarized in Table 1. Each series is composed of three complexes with a single axial halide ligand (L=Cl, Br, I) and one complex with two axial pyridine ligands (L=L′=py). The computational investigation covers all these systems and includes, for comparison, the [FeF(tpfc)] (**8g**) with an axial fluorine ligand and three porphyrin-based iron complexes [Fe-

Table 1. Mössbauer parameters (δ [mm s^{-1}] and ΔE_Q [mm s^{-1}]): Experimental data and B3LYP values computed at optimized B3LYP and BP86 structures.[a]

	S_t	δ_{calcd}	δ_{exptl}	$\Delta E_{Q,calcd}$	$\Delta E_{Q,exptl}$	Electronic structure[b]	DF
1a	3	0.418	0.48	+0.91	1.77	[HS-Fe^{III}P$^{\bullet-}$]$^{2+}$ (F)	B3LYP
	3	0.422		+0.78		[HS-Fe^{III}P$^{\bullet-}$]$^{2+}$ (F)	BP86
2a	2	0.405	0.41	+0.16	0.50	[HS-Fe^{III}P$^{\bullet-}$]$^{2+}$ (AF)	B3LYP
	2	0.388		+0.28		[HS-Fe^{III}P$^{\bullet-}$]$^{2+}$ (AF)	BP86
2b	2	0.408		+0.16		[HS-Fe^{III}P$^{\bullet-}$]$^{2+}$ (AF)	B3LYP
	2	0.295		+2.12		[HS-Fe^{IV}P^{2-}]$^{2+}$	BP86
8g	1	0.194		+2.03		[IS-Fe^{III}(Cor)$^{\bullet 2-}$]$^{+}$	B3LYP
	1	0.141		+2.14		[IS-Fe^{III}(Cor)$^{\bullet 2-}$]$^{+}$	BP86
8a	1	0.181	0.18	+2.45	+2.93[c]	[IS-Fe^{III}(Cor)$^{\bullet 2-}$]$^{+}$	B3LYP
	1	0.125		+2.53		[IS-Fe^{III}(Cor)$^{\bullet 2-}$]$^{+}$	BP86
8d	1	0.175	0.17	+2.61	3.12	[IS-Fe^{III}(Cor)$^{\bullet 2-}$]$^{+}$	B3LYP
	1	0.123		+2.69		[IS-Fe^{III}(Cor)$^{\bullet 2-}$]$^{+}$	BP86
8f	1/2	0.163	0.12	+4.02	3.58	[LS-Fe^{III}(Cor)$^{3-}$]	B3LYP
	1/2	0.118		+3.80		[LS-Fe^{III}(Cor)$^{3-}$]	BP86
9a	1	0.185	0.19	+2.48	2.88	[IS-Fe^{III}(Cor)$^{\bullet 2-}$]$^{+}$	B3LYP
	1	0.132		+2.51		[IS-Fe^{III}(Cor)$^{\bullet 2-}$]$^{+}$	BP86
9d	1	0.180	0.18	+2.63	3.08	[IS-Fe^{III}(Cor)$^{\bullet 2-}$]$^{+}$	B3LYP
	1	0.131		+2.67		[IS-Fe^{III}(Cor)$^{\bullet 2-}$]$^{+}$	BP86
9e	1	0.125	0.15	+2.99	3.35	[IS-Fe^{III}(Cor)$^{\bullet 2-}$]$^{+}$	B3LYP
	1	0.076		+3.04		[IS-Fe^{III}(Cor)$^{\bullet 2-}$]$^{+}$	BP86
9f	1/2	0.162	0.15	+4.04	3.70	[LS-Fe^{III}(Cor)$^{3-}$]	B3LYP
	1/2	0.117		+3.81		[LS-Fe^{III}(Cor)$^{3-}$]	BP86

[a] For each complex, the last column indicates the density functional employed in the geometry optimizations. Experimental data of the porphyrin complexes [Fe(OClO$_3$)$_2$(tpp)] (**1a**) and [FeCl(tpp)]$^+$ (**2a**) were taken from the literature.[23] [b] HS = high spin, LS = low spin, IS = intermediate spin; P = porphyrin, F = ferromagnetic, AF = antiferromagnetic. [c] The signs of the experimental values for ΔE_Q and η are not known, except for complex **8a**.

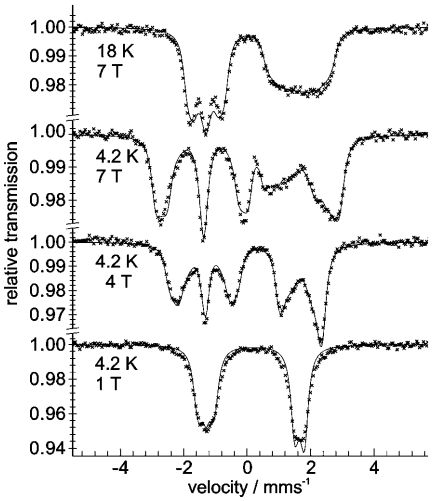

Figure 1. Magnetic Mössbauer spectra of [FeCl(tpfc)] (**8a**) recorded at 4.2 K and 18 K with fields of 1, 4, and 7 T applied perpendicular to the γ-rays. The black lines are the result of a global spin Hamiltonian simulation with $S_t = 1$ and $D_t = 14.1$ cm^{-1}, $E/D_t = 0.07$, $g_t = 2$, $\Delta E_Q = +2.94$ mm s^{-1}, $\eta = 0.2$, $\mathbf{A}/g_N\beta_N = (-24.1, -26.2, +0.5)$ T, and $\delta = 0.18$ mm s^{-1}.

(OClO$_3$)$_2$(tpp)] (**1a**; TPP: *meso*-tetraphenylporphinato) with perchlorato ligands, [FeCl(tpp)]$^+$ (**2a**) and [FeCl(ttp)]$^+$ (**2b**; TTP: *meso*-tetra-*p*-tolylporphinato), which is isoelectronic with **2a**. Experimental Mössbauer parameters are known for the first two of these porphyrin-based complexes,[23] but not for the third one.

To determine the sign and the asymmetry parameter η of the electric quadrupole interaction, as well as the paramagnetic properties for one example of the corrole complexes, magnetic Mössbauer spectra of the chloride complex **8a** were measured at liquid helium temperature with applied fields of 1, 4, and 7 T. The appearance of the spectra shown in Figure 1 is typical of a system with an energetically well-isolated integer-spin ground state with large positive zero-field splitting. In this situation the internal field at the Mössbauer nucleus is weak, because of a low-lying electronic $M_s = 0$ sublevel, and increasing applied fields induce increasing magnetic moments by mixing of M_s levels. This is reflected in the spectra by the relatively weak overall magnetic splitting and the strong field dependence of the hyperfine pattern. These features are consistent with a putative [Fe^{IV}Cl(Cor)$^{3-}$] low-spin complex with $S_{Fe} = 1$ involving the high-valent iron center. However, they could also reflect the alternative [Fe^{III}Cl(Cor)$^{\bullet 2-}$] system containing a corrolato π-radical dianion, with a *total* spin $S_t = 1$ in the ground state, due to strong antiferromagnetic coupling of the intermediate-spin iron ($S_{Fe} = 3/2$) with the corrole-based radical ($S_{Cor} = 1/2$). If the spin coupling is strong, Mössbauer spectroscopy as a ground-state method cannot easily discriminate the two alternatives, because in both cases the ground state is a well-defined spin triplet with basically similar magnetic properties. Conclusions might be drawn only from detailed interpretation of the spin Hamiltonian and Mössbauer parameters.

Given this situation, we tried to simulate the magnetic Mössbauer spectra of **8a** for a low-spin iron(IV) complex with an effective spin $S = 1$. This yields a nice fit with zero-field parameters $D = 14(1)$ cm^{-1}, $E/D = 0.07(5)$ and the hyperfine coupling tensor $\mathbf{A}/g_N\beta_N = -24.1, -26.2, +0.5$ T (black lines in Figure 1). Moreover, the quadrupole interaction is clearly found to be positive with a small asymmetry parameter $\eta = 0.2(1)$. We note that no rotations of the electric field gradient (efg) tensor or the **A** tensor had to be invoked with respect to the principle axes of the zero-field interaction, in contrast to what was reported recently for [Fe^{III}Cl(7,13-Me$_2$Et$_6$Cor)].[17d]

The values can be directly compared with those reported for genuine low-spin iron(IV) species with local spin $S_{Fe} = 1$ at the metal ion. For instance, porphyrin Fe^{IV}–oxo complexes,[1e,f,2] chlorines[2g] and porpholactones[2h] exhibit axial zero-field splitting in the range $19 < D_{Fe} < 36$ cm^{-1}; the value for the non-oxo cation [Fe^{IV}(Ph)porphyrin]$^+$, $D = 31$ cm^{-1}[2i] is also in the same regime, which is slightly higher than the value for **8a**. In contrast, the magnetic hyperfine coupling constant for **8a** is at the lower limit of values found for the same reference compounds, $-25 < A_{Fe,\perp}/g_N\beta_N < -16$ T (here only $A_{Fe,\perp} = 0.5[A_{Fe,x} + A_{Fe,y}]$ is taken, since usually $A_{Fe,x}$ is not very well determined due to the magnetic anisotropy of the spin system).

For the alternative interpretation of **8a** as an $[Fe^{III}Cl(Cor)^{\bullet 2-}]^{+}$ radical complex, the spin Hamiltonian parameters have to be converted to local values referring to the iron spin $S_{Fe}=3/2$. The corresponding relations obtained from spin projection[24] yield $\mathbf{a}_{Fe}=4/5\,\mathbf{A}$; $D_{Fe}=2/3\,D$. The result for **8a** is $\mathbf{a}_{Fe}/g_N\beta_N=-19.3$, -21.0, $+0.4$ T, and $D_{Fe}=9.3\ cm^{-1}$. To our knowledge there are no D and A parameters known for a genuine ferric intermediate-spin porphyrin.[25] The values obtained for **8a** compare rather well with those found for the penta-coordinate N_4-macrocyclic complex[26] $[Fe^{III}Cl(\eta_4\text{-MAC})]^{2-}$ (H_4[MAC]=1,4,8,11-tetraaza-13,13-diethyl-2,2,5,5,7,7,10,10-octamethyl-3,6,9,12,14-pentaoxocyclotetradecane) and the iodoiron(III) [N_4]macrocycle of Jäger[27] with $-3.7\le D_{Fe}\le 13\ cm^{-1}$ and $-12.7<a_{Fe,\perp}/g_N\beta_N<-22$ T. An example of a non-porphyrin monoradical system is the intermediate-spin complex $[Fe^{III}(L^{ISQ})(L^{PDI})$(BuPhCH-py)] with *N*-phenyl-*o*-diiminobenzosemiquinonate (L^{PDI}) and *o*-iminothionebenzosemiquinonate (L^{ISQ}) ligands.[28] It also has a total spin $S=1$ ground state with large zero-field parameters $D=48\ cm^{-1}$, $E/D=0.2$, and a magnetic hyperfine coupling tensor $\mathbf{A}/g_N\beta_N=-13.4$, -39.6, $+0$ T. The very large D value in the last example is quite remarkable, but in spite of the very different ligand system, the basic features of large zero-field splitting and anisotropic **A** tensor resemble those of our compound [FeCl(tpfc)] (**8a**).

In summary, neither the iron(IV) nor the alternative iron(III)–radical interpretation can be clearly ruled out from the spin-Hamiltonian parameters obtained for **8a** without explicit quantum chemical calculations. However, temperature and field-dependent magnetization measurements, as shown in Figure 2, not only corroborate the zero-field splitting of the electronic ground state of **8a**, but also provide strong evidence for the presence of a spin-coupled iron(III)–radical system. Global simulation of the curves for the effective magnetic moment $\mu_{eff}(T)$ and the multifield data recorded for the molar magnetization, $M(g\mu_B(kT)^{-1})$ with two exchange-coupled spins $S_{Fe}=3/2$, $S_{Cor}=1/2$ yields $D_{Fe}=9.5(2)\ cm^{-1}$, $E/D_{Fe}=0(0.05)$, $g_{Fe}=2.058$, and $J=-272(10)\ cm^{-1}$. The last value is obtained from the small but distinct increase of $\mu_{eff}(T)$ above 200 K, which indicates thermal population of the excited, total-spin quintet state that must exist for a $[Fe^{III}Cl(Cor)^{\bullet 2-}]^{+}$ system. We emphasize that the particular rise of the experimental data cannot be attributed to temperature-independent paramagnetism (TIP), since subtraction of TIP will lead to a wrong (negative) slope for the data in the range 50–200 K. To our knowledge this is the first time that such an increase of the effective magnetic moment has been observed for an iron corrole complex. We take it as a direct probe for the corrolate π-radical.

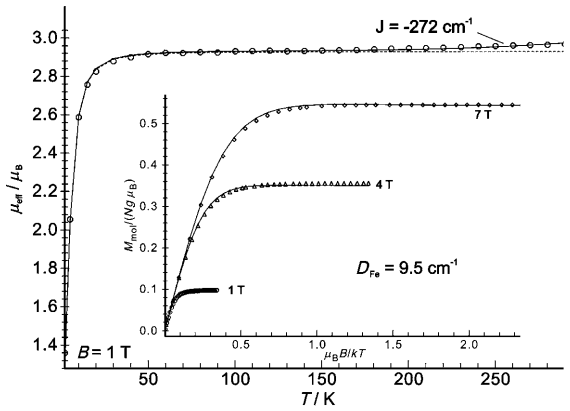

Figure 2. Effective magnetic moment $\mu_{eff}(T)$ of [FeCl(tpfc)] (**8a**) recorded with $B=1$ T and multifield measurement of the molar magnetization (inset). The solid lines are the result of a global spin Hamiltonian simulation with $S_{Fe}=3/2$, $S_{rad}=1/2$, $D_{Fe}=9.5\ cm^{-1}$, $E/D_{Fe}=0$, $g_{Fe}=2.058$, $g_{rad}=1/2$, and $J=-272\ cm^{-1}$. The grey dotted line marks the limit of strong antiferromagnetic exchange with $J\rightarrow\infty$.

The small Mössbauer isomer shifts ($\delta=0.15$–$0.19\ mm\,s^{-1}$,) and large quadrupole splitting ($\Delta E_Q=+2.88$–$3.58\ mm\,s^{-1}$) of the corrolate complexes (Table 1) are at the very high end of what is expected for genuine triplet iron(IV) species, but also consistent with the assignment of the electronic structure as $[Fe^{III}Cl(Cor)^{\bullet 2-}]$. They are in the range found for other iron(III) compounds with unambiguously approved intermediate-spin state, like the archetypical dithiooxalatoiron(III) halides ($\delta=0.25$–$0.30\ mm\,s^{-1}$, $\Delta E_Q=+3.25$–$3.60\ mm\,s^{-1}$),[30] the iodoiron(III) [N_4]macrocycle[27] ($\delta=0.18\ mm\,s^{-1}$, $\Delta E_Q=+3.56\ mm\,s^{-1}$), and the macrocyclic dianion $[Fe^{III}Cl(\eta_4\text{-MAC})]^{2-}$ ($\delta=0.25\ mm\,s^{-1}$, $\Delta E_Q=+3.60\ mm\,s^{-1}$),[31] but also with diradical iron(III) halide complexes of the type $[Fe^{III}(L^{ISQ})_2(L)]$ (L=Cl, Br, or I) with *N,S*-coordinating *o*-iminothionebenzosemiquinonate (L^{ISQ}) ligands and total spin $S_t=1/2$ ($\delta=0.15$–$0.17\ mm\,s^{-1}$, $\Delta E_Q=+2.97$–$3.09\ mm\,s^{-1}$),[32] and the monoradical complex $[Fe^{III}(L^{ISQ})(L^{PDI})$(BuPhCH-py)] ($\delta=0.20\ mm\,s^{-1}$, $\Delta E_Q=+3.06\ mm\,s^{-1}$).[33] These all compare quite well with compound **8a**.

Geometries: Table 2 lists selected structural parameters from the B3LYP and BP86 optimized geometries and from the available X-ray data. In general, the B3LYP and BP86 calculations converge to the same electronic configuration and yield rather similar geometries. The only exception is $[FeCl(ttp)]^{+}$, for which the two density functionals predict

Table 2. Comparison of the optimized structural parameters with available X-ray data.

	S_t	Fe–N1[a]	Fe–N2[a]	Fe–L	Δ[b]	Source
1a	3	2.04	2.05	2.13		exptl[23]
	3	2.073	2.085	2.084	0	B3LYP
	3	2.077	2.092	2.076	0	BP86
2a	2	2.102	2.104	2.208	0.498	B3LYP
	2	2.098	2.068	2.203	0.464	BP86
2b	2	2.09	2.05	2.168		exptl[23]
	2	2.103	2.100	2.210	0.498	B3LYP
	2	1.991	1.992	2.258	0.291	BP86
8g	1	1.917	1.948	1.817	0.417	B3LYP
	1	1.900	1.927	1.783	0.396	BP86
8a	1	1.881	1.921	2.238	0.367	exptl[18]
	1	1.913	1.944	2.252	0.416	B3LYP
	1	1.897	1.924	2.185	0.389	BP86
8d	1	1.910	1.941	2.412	0.402	B3LYP
	1	1.895	1.922	2.338	0.379	BP86
8e	1	1.896	1.926	2.624	0.372	B3LYP
	1	1.881	1.909	2.526	0.353	BP86
8f	1/2	1.865	1.923	2.030	0.001	exptl[10e]
	1/2	1.891	1.931	2.100	0.065	B3LYP
	1/2	1.883	1.924	2.045	0.064	BP86
9a	1	1.914	1.943	2.264	0.418	B3LYP
		1.898	1.926	2.192	0.398	BP86
9d	1	1.911	1.940	2.424	0.407	B3LYP
	1	1.896	1.923	2.346	0.388	BP86
9e	1	1.896	1.925	2.639	0.374	B3LYP
	1	1.883	1.909	2.536	0.358	BP86
9f	1/2	1.892	1.931	2.098	0.067	B3LYP
	1/2	1.883	1.925	2.040	0.065	BP86

[a] Fe–N1 and Fe–N2 are the average bond lengths of two Fe–N bonds in Å. [b] Distances of the iron center out of the plane defined by N4 core.

qualitatively different electronic structure (vide infra) and therefore also very different geometries, with deviations of about 0.1 Å in the iron–ligand distances and about 0.2 Å in the out-of-plane coordinate of iron. If the special case of $[FeCl(ttp)]^+$ is excluded, the discrepancies between the B3LYP and BP86 bond lengths become much smaller, especially in the case of the remaining two porphyrins. Compared to BP86, the B3LYP functional tends to predict somewhat larger iron–ligand distances for the corroles, with differences of 0.03 Å for the equatorial Fe–N bonds and typically 0.05–0.10 Å for the axial Fe–L bonds.

The better match with the experimental X-ray structure indicates that B3LYP identifies the correct electronic configuration for $[FeCl(ttp)]^+$. In the case of the porphyrin complex $[Fe(OClO_3)_2(tpp)]$, the B3LYP and BP86 geometries are almost identical, but both differ appreciably from the X-ray structure: the equatorial Fe–N bonds are elongated by about 0.04 Å, while the axial Fe–O bonds are contracted by 0.05 Å. For the two currently studied corrole complexes with known X-ray structures (**8a**, **8f**), both B3LYP and BP86 reproduce the experimental Fe–N bond distances quite well, but there are larger deviations from experiment for the axial iron-ligand bonds (up to 0.07 Å for $[Fe(py)_2$-(tpfc)] in B3LYP, see Table 2).

Calculation of the Mössbauer parameters: The computed isomer shifts (δ) and quadrupole splittings (ΔE_Q) are given in Table 1 and are compared to the experimentally available data. The theoretical values are known to have method specific uncertainties of typically up to $\leq 0.1\ mm\,s^{-1}$[34] and $\leq 0.5\ mm\,s^{-1}$,[35] respectively. The calculated isomer shifts thus agree reasonably well with experiment, since all deviations are well below $0.1\ mm\,s^{-1}$. In the case of quadrupole splittings, most of the deviations from experiment also remain within the expected limits. However, a large discrepancy is found for $[Fe(OClO_3)_2(tpp)]$, in which the difference between calculated (B3LYP geometry) and experimental ΔE_Q is $0.86\ mm\,s^{-1}$. This may be due to the fact that perchlorate is a very weak ligand, and it is thus difficult to predict its bonding interaction with the iron center accurately. This is also evidenced in the geometric parameters for this complex (Table 2): Experimentally, the Fe–L bond (2.13 Å) is significantly longer than the Fe–N bonds (2.04–2.05 Å), whereas these bonds are essentially equidistant in the calculations. Clearly any disorder in the structure of such weakly coordinating anions will affect the quadrupole splitting more strongly than the isomer shift.

In the halogenoiron corrole complexes, the Mössbauer parameters computed at the B3LYP geometries are generally close to experiment, whereas those computed at the BP86 geometries exhibit slightly larger deviations from experiment. In the former case (B3LYP geometries) the isomer shifts are typically within $0.02\ mm\,s^{-1}$ of the experimental values, while the quadrupole splittings are underestimated by ≈ 0.4–$0.5\ mm\,s^{-1}$, but show the right variation within each halide series (see Table 1). These results give us confidence that the calculations have converged to the correct electronic states, since the spectroscopic parameters are more sensitive to the electronic structure than the total energy itself.[36]

To investigate the influence of the employed Hamiltonians (non-relativistic vs. relativistic) on the calculated Mössbauer parameters, a test calculation on [FeBr(tpfc)] was performed by using the ZORA Hamiltonian. However, it turned out that essentially identical results were obtained between the relativistic and non-relativistic calculations ($\delta =$ 0.157 vs. $0.175\ mm\,s^{-1}$, $\Delta E_Q = 2.69$ vs. $2.61\ mm\,s^{-1}$ and $\eta =$ 0.04 vs. 0.03). Hence, the remaining calculations were done without relativistic corrections.

Electronic structure—orbital analysis

*$[Fe(OClO_3)_2(tpp)]$ (**1a**) ($S_t = 3$)*: The molecular orbital diagram for **1a** (Figure 3) shows that there are five singly occupied MOs that are all metal-centered, while the sixth spin-up SOMO is a porphyrin π orbital. This pattern results in a septet ground state with ferromagnetic coupling between the high-spin ferric metal center ($S_{Fe} = 5/2$) and a porphyrin anion radical ($S_P = 1/2$) in agreement with the local effective D_{4h} symmetry of the iron center.[23]

*$[FeCl(tpp)]^+$ (**2a**) ($S_t = 2$)*: The electronic structure of **2a** may be described either as a high-spin ferric ion ($S_{Fe} = 5/2$)

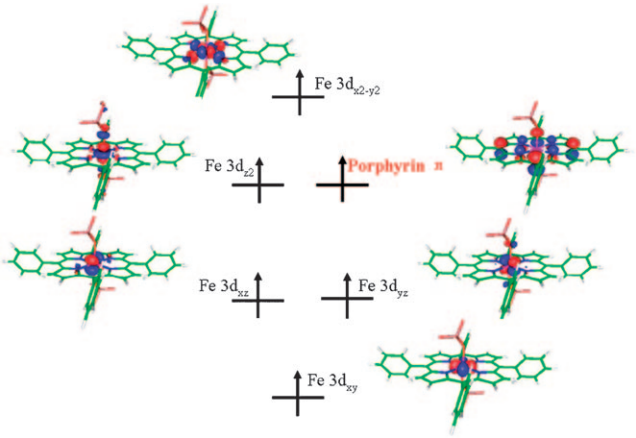

Figure 3. Schematic MO diagram for $[Fe(OClO_3)_2(tpp)]$ (**1a**); quasi-restricted orbitals were used.

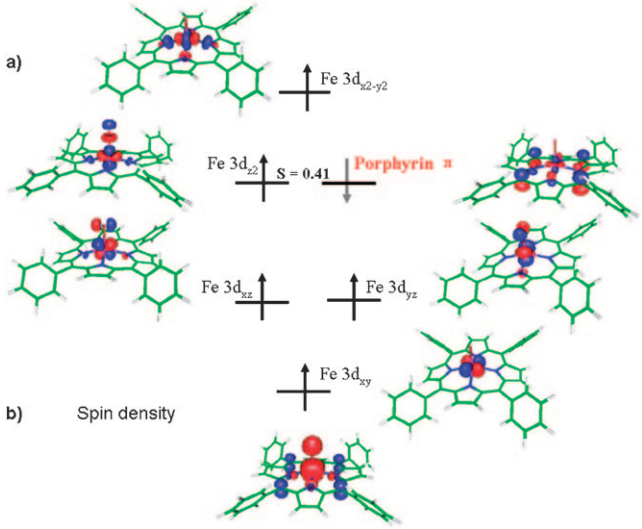

Figure 4. a) Schematic MO diagram and spin density for $[FeCl(tpp)]^+$ (**2a**); the spin-coupled pair represents unrestricted corresponding orbitals, whereas for the remaining orbitals quasi-restricted orbitals were employed. b) Spin density plot of $[FeCl(tpp)]^+$.

antiferromagnetically coupled to a porphyrin radical anion ($S_P = 1/2$) (BS(5,1)); or as a high-spin iron(IV) center chelated by a porphyrin dianion (BS(4,0)). Both initial guesses eventually converged to the BS(5,1) solution for both density functionals. The MOs of **2a** (Figure 4) from this solution closely resemble those of **1a** except that an electron with opposite spin resides in the porphyrin π orbital. This forms a spin-coupled pair with the Fe d_{z^2} orbital by means of a π pathway with a considerable mutual spatial overlap of $S = 0.41$. This situation is best described as antiferromagnetic coupling between high-spin iron(III) and a porphyrin radical.

*$[FeCl(TTP)]^+$ (**2b**) ($S_t = 2$)*: In analogy to **2a**, two possible electronic solutions BS(5,1) and BS(4,0) for **2b** were evaluated. We found that, using the B3LYP functional the electronic structure converged to the BS(5,1) solution while using the BP86 functional the BS(4,0) solution was obtained. The BS(4,0) spin state was calculated by the B3LYP functional, at the BP86 geometry, and found to be slightly higher in energy (6.3 kcal mol^{-1}) than the broken-symmetry state BS(5,1).

A qualitative molecular orbital diagram computed from the BS(5,1) and BS(4,0) solutions is presented in Figure 5. The BS(5,1) configuration for **2b** is similar to that for **2a**,

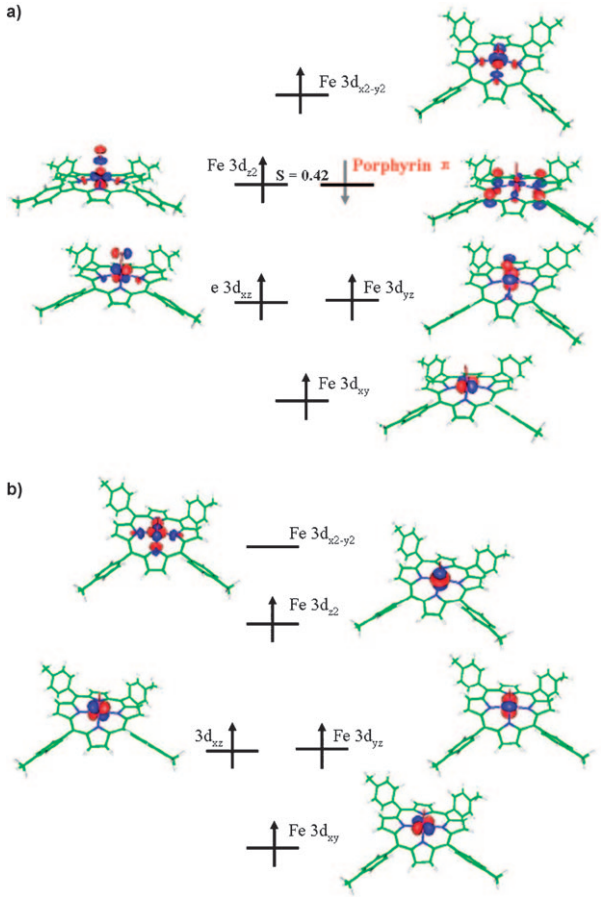

Figure 5. Schematic MO diagram for $[FeCl(ttp)]^+$ (**2b**) derived from a) BS(5,1) and b) BS(4,0); the spin-coupled pair represents corresponding orbitals, whereas for the remaining orbitals quasi-restricted orbitals were employed.

best described as a high-spin ferric center ($S_{Fe} = 5/2$) antiferromagnetically coupled to a porphyrin radical ligand ($S_P = 1/2$). For the BS(4,0) solution, the unpaired electrons reside in four metal-based d orbitals with the strongly σ-antibonding $d_{x^2-y^2}$ orbital being unoccupied to yield a quintet state. Thus it should be best interpreted as a high-valent high-spin ferryl species.

The clear difference in the isomer shift and quadrupole splitting values for these two distinct electronic configurations implies that these parameters are able to clearly distinguish between the different electronic states. A Mössbauer experiment on **2b** should thus allow the assignment of the

ground state through comparison with the computed Mössbauer parameters. We note in this context that the isomer shift is a more critical discriminator of the electronic structure, because it can be calculated more reliably. We anticipate a BS(5,1) electronic structure for this species because the B3LYP geometry for this configuration is much closer to the experimental geometry than the BP86 geometry for the BS(4,0) configuration.

*[Fe(L)(tpfc)] (**8a**, **8d**, **8e**, **8g**) and [Fe(L)(tdcc)] (**9a**, **9d**, **9e**) (L=F, Cl, Br, I) (S_t=1)*: These complexes attracted intense interest in the bioinorganic chemistry community, because they may serve as the model compounds for compound II in porphyrin chemistry. The electronic structure of these complexes may be assigned either as a high-valent ferryl species with trianionic corrole ligand, like compound II, or a ferric species antiferromagnetically coupled to a dianionic radical ligand. Therefore, two different initial estimates for the electronic structure, namely BS(2,0) ([LS-Fe^{IV}-$(Cor)^{3-}$]$^+$) and BS(3,1) ([IS-$Fe^{III}(Cor)^{\bullet 2-}$]$^+$) were tested (LS=low spin; IS=intermediate spin). However, the BS-(2,0) structure always converged to the BS(3,1) solution.

A molecular orbital diagram obtained from the optimized structure of **8a** by using the B3LYP functional is presented in Figure 6a. Analogous results were obtained with the BP86 functional. In the upper valence region one can identify one doubly occupied and three singly occupied metal-based d orbitals in the spin-up manifold and one corrole a_{2u}-like π orbital in the spin-down manifold. Spin coupling is exhibited through a π pathway involving the Fe d_{z^2} and corrole π orbitals with a substantial mutual spatial overlap of S= 0.52. This orbital occupation pattern is best interpreted as an intermediate-spin ferric center (S_{Fe}=3/2) antiferromagnetically coupled to a dianionic radical ligand (S_{cor}=1/2). The oxidation of the corrole ring is also observable in the spin-density plot (Figure 6b). The sum of the spin populations on the corrole ligand amounts to ≈0.8 unpaired electrons, while 2.7 unpaired electrons reside on the iron halide core, which is in agreement with previous DFT calculations employing the same density functional.[17d] Similar results were obtained for fluoro-, bromo- and iodo-analogues indicating that these three complexes have analogous electronic structures as is also indicated by the similar Mössbauer parameters.

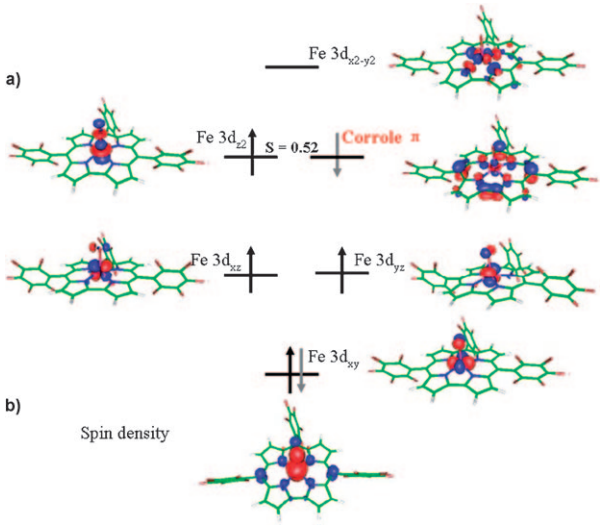

Figure 6. a) Schematic MO diagram and spin density for [FeCl(tpfc)] (**8a**); the spin-coupled pair represents unrestricted corresponding orbitals, whereas for the remaining orbitals quasi-restricted orbitals were employed. b) Spin density plot of **8a**.

*[Fe(py)$_2$(tpfc)] (**8f**) and [Fe(py)$_2$(tdcc)] (**9f**) (S_t=1/2)*: Similar to **8a**, two different solutions, namely, BS(1,0) ([LS-Fe^{III}-$(Cor)^{3-}$]) and BS(2,1) ([LS-$Fe^{II}(Cor)^{\bullet 2-}$]) were attempted. However, all calculations converged to the "pure" spin solution BS(1,0) irrespective of the adopted density functional. A qualitative molecular-orbital diagram computed from the BS(1,0) approach is presented in Figure 7. Two metal-based t_{2g} orbitals, d_{xy} and d_{yz}, are doubly occupied, while one is singly occupied; the two antibonding e_g orbitals are unoccupied. This leads to a doublet ground state with a low-spin iron(III) atom coordinated to a fully reduced corrole ligand.

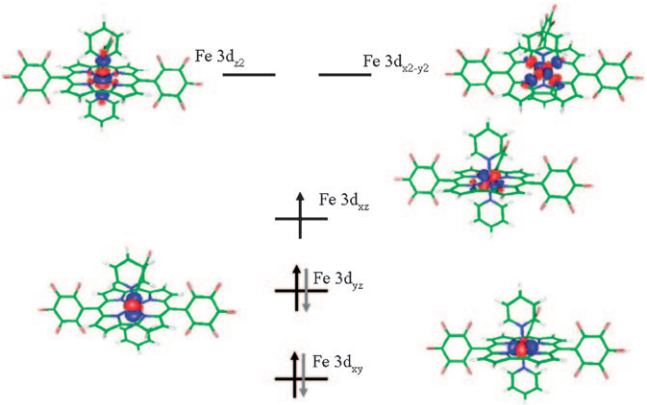

Figure 7. Schematic MO diagram for [Fe(py)$_2$(tpfc)] (**8f**); quasi-restricted orbitals were employed.

Discussion

In this work we have presented a combined experimental (Mössbauer) and theoretical (DFT) approach to differentiate between the two possible electronic structure descriptions for halogenoiron corroles, particularly for those containing electron-withdrawing corroles. The reasonable agreement of the predicted Mössbauer parameters with the experimental spectroscopic data implies that the calculations have converged to electronic states compatible with the actual molecular ground states. Further detailed analysis of the obtained Kohn–Sham solutions then allows for a more detailed insight into the electronic structure. Before presenting our conclusions, previous work on these two aspects will be briefly discussed.

Mössbauer data: Mössbauer spectroscopy has been employed in the past to investigate chloroiron corroles.[16,17d] While the observed isomer shifts are very different from the high-spin iron(III) porphyrin radical complexes (Table 1), they fall into the region that is intermediate between those typical for intermediate-spin iron(III) ($S=3/2$) and low-spin iron(IV) ($S=1$). This prevented definitive electronic structure conclusions to be drawn.

DFT calculation and electronic structure: DFT calculations on chloroiron corroles (**5a**, **6a**, **7a**) favored the formulation as $[IS\text{-}Fe^{III}(Cor)^{\bullet 2-}]^{+}$ due to the large negative spin population calculated on the *meso*-carbon atoms. The calculated spin populations on iron varied between 2.0[20b] and 2.6 in different reports,[17d] which is intermediate between the values expected for triplet iron(IV) and quartet iron(III). The apparent differences may be ascribed to the employed density functional: pure GGA density functionals like PW91 used by Ghosh et al.[20b] tend to overestimate metal–ligand covalency, leading to reduced spin populations on the metal center, while hybrid density functionals such as B3LYP employed by Walker, Trautwein, and co-workers[17d] provide more ionic bonds. More importantly, however, individual atomic or orbital spin and charge populations are not observables in the strict quantum mechanical sense. Thus deciphering the electronic structure from the spin density profile and/or spin population may not be fully reliable. Moreover, the question whether the correct electronic solution for a given compound was obtained cannot be addressed by such calculations without seeking experimental feedback. According to our experience, spectroscopic properties are more sensitive to the electronic structure than total energies (e.g., see reference [36]). Thus, comparison of the calculated spectroscopic parameters with those derived from experiment is essential for the assignment of the electronic structure in the investigated systems.

Exchange coupling: For the analysis of the obtained Kohn–Sham solutions in terms of more familiar chemical terms, the corresponding orbital transformation was used in this work. As discussed elsewhere,[37] pairs of corresponding orbitals with spatial overlap close to 1 represent doubly occupied orbitals; those with spatial overlap significantly less than 1 correspond to "magnetic orbitals". This allows a pictorial approach to antiferromagnetic coupling pathways. Moreover, the spatial overlap of the magnetic corresponding orbital pairs provides a measure for the strength of the antiferromagnetic interaction as demonstrated in Table 3.

One outcome of the current investigations is that the exchange interaction in the corrole systems is much stronger than that in the porphyrin analogues (first two entries in Table 3). Inspection of the magnetic orbitals in the corrole and porphyrin systems shows that they have analogous nodal structures; hence symmetry-based arguments are unlikely to be responsible for the differences. However, the absence of one *meso*-carbon atom renders the corrole cavity rather small, as evidenced by the shorter Fe–N bond lengths in the corrole systems, which could be responsible for the stronger metal–macrocycle interactions. The Fe d_{z^2} orbital contributions are nearly identical in the spin-up magnetic orbital for both systems, but the contributions from the four coordinating nitrogen atoms are slightly larger in the corrole system than those in the corresponding porphyrin system (18% vs. 12%) in the spin-down magnetic orbital.

Table 3. Calculated exchange coupling constants and mutual spatial overlaps in the spin coupled pair (B3LYP values at optimized B3LYP geometries).

	J [cm^{-1}]	Spatial overlap		J [cm^{-1}]	Spatial overlap
2a	−263	0.41	**8g**	−580	0.46
2b	−267	0.42	**9a**	−665	0.51
8a	−664	0.52	**9d**	−687	0.54
8d	−691	0.54	**9e**	−739	0.60
8e	−766	0.61			

The question of how reliable the calculated exchange couplings are is difficult to answer. For [Fe(tpp)Cl], our calculations are consistent with the experimental estimate ($|-2J| \geq 500\ cm^{-1}$).[23] In the present work, we have observed features in the susceptibility of [FeCl(tpfc)] which suggest that the calculated exchange coupling constant is overestimated by about a factor of two. This arises from the fact that based on the calculated exchange coupling constant we should not have been able to observe an excited quintet state as we did experimentally. However, a more focused experimental investigation of a series of complexes appears to be necessary in order to settle this point convincingly. Although this is outside the scope of the present work, we note that there are indeed many indications that the binding of metal ions by corroles is much more covalent than by porphyrins.[15] A chemical indication for the less ionic bonding of metal ions by corroles is that acid-induced demetalation is a rare phenomenon in corrole chemistry.

Comparison of corrole and porphyrin systems: To gain further insight into the exchange interaction, a rigid surface scan of the out-of-plane distance of the iron center relative to the macrocyclic plane was carried out for [FeCl(Cor)] and $[FeCl(Por)]^{+}$. The results (Figure 8) indicate that the overlap of the magnetic orbitals increases up to a maximum and then decreases again with increasing out-of-plane distance. The trend in the fragment–fragment overlap is consistent with the calculated potential-energy surface curve, since the minimum occurs very close to the position of maximum iron–ligand overlap. For the porphyrin system, it is known that the HOMO and HOMO−1 are nearly (accidentally) degenerate and transform under a_{2u} and a_{1u} in D_{4h} symmetry, while the iron d_{z^2} orbital transforms as a_{1g}. For the five-coordinate complexes that we studied here the relevant point groups are C_{4v} (porphyrin) and C_s (corrole). In this case there are no symmetry restrictions for the mixing of the iron d_{z^2} and at least one of the high-lying corrole or porphyrin orbitals (a group theoretical analysis of the fragment-orbital interactions is contained in the Supporting Information).

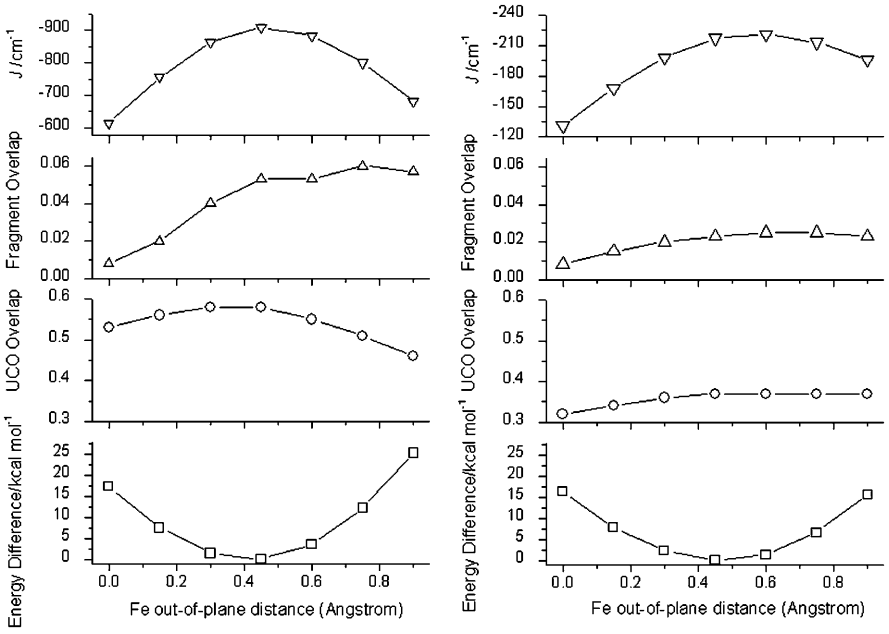

Figure 8. Evolution of the ligand–metal exchange coupling, the metal–ligand fragment–fragment overlap, the corresponding orbital overlap, and the total broken-symmetry DFT energy for hypothetical planar [FeCl(corrole)] (left) and [FeCl(porphyrin)]$^+$ (right) as function of the iron out-of-plane distance.

Nevertheless, if the iron is in the plane of the hypothetical ligands, the fragment–fragment overlap is still zero due to the nodal structure of the orbitals that are involved. However, even at this point there is still kinetic exchange that leads to antiferromagnetic coupling. Upon moving the iron out of the plane, the HOMO and HOMO−1 of the porphyrin transform as a_1 and a_2, respectively, while the iron d_{z^2} transforms as a_1. Hence, if the magnetic orbital on the porphyrin is a_1 there is a nonzero fragment–fragment overlap and the antiferromagnetic coupling increases (in magnitude) up to a certain point at which it passes through a maximum. This just mirrors the behavior of the fragment–fragment overlap.

For the corrole system the situation is quite similar, although the metal–ligand overlap is always allowed. Here, the iron and the magnetic corrole orbital have a nonzero overlap throughout and the overall interaction between the ring and the iron is much stronger than in the porphyrin case with J maximizing (in magnitude) at a similar out-of-plane distance.

There is, however, another very important difference between the corrole and porphyrin systems: in the porphyrin, the iron is locally in a high-spin state ($S_{Fe}=5/2$), while in the corrole the iron has intermediate spin ($S_{Fe}=3/2$). The reason for this is the much stronger σ-interaction in the corrole that makes the $d_{x^2-y^2}$ orbital energetically unavailable. As a result of the high-spin configuration, the occupied spin-up orbitals in the iron porphyrin are much more strongly stabilized by spin polarization than the corresponding corrole orbitals (note that the energy difference of the metal d and the highest occupied macrocyclic π orbitals is ≈3 eV in the corrole complex and ≈7 eV in the porphyrin system; see the Supporting Information). Hence, the interaction of the iron d orbitals with the ring orbitals is much stronger in the spin-up as well as the spin-down manifold in the corrole system.

Spin population: When comparing the fragment spin populations, one can identify considerable negative spin population on the four coordinating N atoms (−0.27) and three *meso*-carbons (−0.50) in the corrole systems, while in the case of the porphyrin systems most of the negative spin population (≈−0.68) is localized on the four *meso*-carbon atoms and only a very small fraction (−0.04) resides on the coordinating N atoms. This can be traced back to the exceptionally strong metal–ligand σ interactions in corrole systems.[14] They render the Fe $d_{x^2-y^2}$ orbital too high in energy to be occupied and thus yield an intermediate-spin state for the iron center ($S_{Fe}=3/2$) in the electronic ground state. By contrast, this orbital is singly occupied in the corresponding porphyrin system in which the iron center locally exists in a high-spin state ($S_{Fe}=5/2$). The strongly antibonding $d_{x^2-y^2}$-based orbital induces positive spin density in the σ system of the porphyrin ring that counteracts the negative spin density that resides in the π system due to the open-shell nature of the porphyrin ligand. Since a similar compensation does not take place in the corrole system, it has more negative unpaired spin population residing on the coordinating nitrogen atoms.

Conclusion

In this work a combined experimental and theoretical approach was employed to investigate [Fe(L)(Cor)] (L = F, Cl, Br, I, Cor = TPFC, TDCC) complexes **8a**, **8d–f**, **9a**, and **9d–f** containing strongly electron-deficient corrole ligands. Although these substituents significantly change the redox properties of the complexes, our results indicate that the electronic structures are analogous to those calculated for the unsubstituted chloroiron corroles with electron-rich corrole ligands, in line with the studies on the chloroiron β-octafluorocorrole complex.[38] Mössbauer spectroscopy alone is not able to unambiguously discriminate between the two alternative formulations: low-spin iron(IV) chelated by a closed-shell corrolato trianion versus intermediate-spin iron(III), which is strongly antiferromagnetic coupled with a

corrolato π-radical dianion. However, the combination of the Mössbauer data with electronic structure calculations provides strong evidence for preferring the latter intermediate-spin iron(III) description. We have provided additional support for this formulation by the detailed interpretation of the spin Hamiltonian and Mössbauer parameters that were obtained in this work. Further experimental evidence for a spin-coupled iron(III)–radical system was provided by temperature and field-dependent magnetization measurements that revealed a small but distinct increase of $\mu_{eff}(T)$ above 200 K, indicative of thermal population of the excited total spin quintet state.

After establishing that the DFT calculations are in agreement with the available experimental data, a detailed analysis of the obtained Kohn–Sham solutions in terms of corresponding orbitals provided insight into the electronic structures of the investigated systems. The analysis revealed that similar orbitals (Fe d_{z^2} orbital and the highest occupied a_{2u}-like π orbital of the ring) are involved in magnetic coupling in the iron porphyrin- and corrole-based systems, and that the coupling in the latter case is much stronger. A key difference between the porphyrin- and corrole-based systems is that in the former the iron is locally in a high-spin $S_{Fe}=5/2$ state, while in the latter the macrocycle–iron σ bonds become so strong that the iron is forced into an intermediate-spin $S_{Fe}=3/2$ configuration. The resulting consequences for the magnetic properties of these systems have been explored in some detail in this work. Possible implications for their reactivity will be addressed in future studies.

Experimental Section

Magnetic susceptibility data were measured from powder samples of solid material in the temperature range 2–300 K using a SQUID susceptometer (MPMS-7, Quantum Design) with a field of 1.0 T. Multiple-field variable-temperature magnetization magnetization equidistantly sampled on a T^{-1} temperature scale. The experimental data were corrected for underlying diamagnetism by use of tabulated Pascal's constants, as well as for temperature-independent paramagnetism. The susceptibility and magnetization data were simulated with our own package julX for exchange-coupled systems written by E.B. The simulations are based on the usual spin-Hamilton operator for exchange-coupled paramagnetic systems of intermediate-spin iron(III) and a ligand radical with spins $S_{Fe}=3/2$ and $S_{rad}=1/2$ [Eq. (1)].

$$H = -2J\vec{S}_{Fe}\cdot\vec{S}_{rad} + \mu_B(g_{Fe}\vec{S}_{Fe} + g_{rad}\vec{S}_{rad})\vec{B} + D_{Fe}[S^2_{Fe,z} - {}^1/_3 S_{Fe}(S_{Fe}+1) + \frac{E_{Fe}}{D_{Fe}}(S^2_{Fe,x} - S^2_{Fe,y})] \quad (1)$$

In Equation (1) g_i is the local electronic g value, and D_{Fe} and E_{Fe}/D_{Fe} are the axial zero-field splitting and rhombicity parameters of the ferric ion. The magnetic moments were obtained from the first-order derivative of the eigenvalues of Equation (1). Powder summations were done by using a 16-point Lebedev grid.

Mössbauer data were recorded on a spectrometer with alternating constant acceleration. The minimum experimental line width was 0.24 mm s^{-1} (full width at half-height). The sample temperature was maintained constant either in an Oxford Instruments Variox or an Oxford Instruments Mössbauer-Spectromag cryostat, which is a split-pair super-conducting magnet system for applied fields up to 8 T in which the temperature of the sample can be varied in the range 1.5 to 250 K. The field at the sample is perpendicular to the γ-beam. The ^{57}Co/Rh source (1.8 GBq) was positioned at room temperature inside the gap of the magnet system at a zero-field position. Isomer shifts are quoted relative to iron metal at 300 K.

Magnetic Mössbauer spectra were simulated by using the electronic spin-Hamiltonian for the total spin $S_t=1$ of the system [Eq. (2)] together with the usual nuclear Hamiltonian for the hyperfine interactions of the ^{57}Fe nuclei [Eq. (3)], for which $\vec{I}\mathbf{A}\vec{S}_t$ is the magnetic hyperfine coupling that connects S_t and the nuclear spin I, and $\mathbf{A}$ is the hyperfine coupling tensor.

$$H = g\beta\vec{S}_t\cdot\vec{B} + D_t[S^2_{t,z} - 2/3 + E/D_t(S^2_{t,x} - S^2_{t,y})] \quad (2)$$

$$H_{nuc} = \vec{I}\mathbf{A}\vec{S}_t - g_N\beta_N\vec{I}\vec{B} + H_Q \quad (3)$$

The nuclear quadrupole interaction is given by Equation (4) in which Q is the quadrupole moment, and V_{zz} and η are the main component and the asymmetry parameter of the electric field gradient tensor, respectively.

$$H_Q = \frac{eqQV_{zz}}{4I(2I-1)}[3I_z^2 - I^2 + \eta(I_x^2 - I_y^2)] \quad (4)$$

The corresponding quadrupole splitting as observed in zero-field spectra is given by Equation (4). The isomer shift δ was just added to the Mössbauer transition energies.

Computational methods: All computations in this work were carried out with the ORCA program package.[39] Geometry optimizations for all the complexes were performed with the BP86[40] and B3LYP[41] density functional. The TZVP[42] (Fe, O, N and the halide atoms in the first coordination sphere), and SV(P) (other elements) basis sets[43] were applied in combination with the auxiliary basis sets TZV/J (Fe, O, N, and coordinating halide atoms) and SV/J.[44] The RI[44,45] and RIJONX[46] approximations were used to accelerate the calculations. Because several broken symmetry solutions to the spin-unrestricted Kohn–Sham equations may be obtained for many of the compounds in this work, the general notation BS(m,n)[47] has been adopted, in which m (n) denotes the number of unpaired spin-up (spin-down) electrons at the two interacting fragments.

Spectroscopic parameters: The spectroscopic data were obtained from additional single-point calculations. For that purpose, the B3LYP hybrid density functional was applied in combination with the CP(PPP)[34] basis set for Fe, and the TZVP basis set for the nitrogen, oxygen, and halide atoms in the first coordination sphere. The SV(P) basis set was used for the remaining atoms. The nature of the solution was investigated by the corresponding orbital transformation,[47] which, through the corresponding orbital overlaps, demonstrates whether the system is to be described as a spin-coupled or a normal almost spin-pure Kohn–Sham determinant.

Quadrupole splittings (ΔE_Q) were obtained from electric field gradients V_i ($i=x$, y, z) by employing a nuclear quadrupole moment, Q(^{57}Fe), of 0.16 barn [Eq. (5)]:[48]

$$\Delta E_Q = {}^1/_2 eQV_{zz}\sqrt{1 + {}^1/_3\eta^2} \quad (5)$$

Here, $\eta=(V_{xx}-V_{yy})/V_{zz}$ is the asymmetry parameter of the nuclear quadrupole tensor. Isomer shifts (δ) were calculated from the electron densities at the Fe nuclei (ρ_0) by employing the fit equation [Eq. (6)] in which C is a constant of 11800 au^{-3}, and $a=-0.367$ au^3 mm s^{-1} and $b=+6.55$ mm s^{-1} are the fit parameters from our previous work.[48]

$$\delta = \alpha(\rho_o - C) + b \quad (6)$$

For iodine complexes, the scalar relativistic zero'th order regular approximation (ZORA) Hamiltonian was employed for geometry optimizations

and Mössbauer parameter calculations in conjunction with newly contracted ZORA basis sets.[49] For ZORA calculations, a new calibration curve for isomer shifts was established ($C = 13770\ \mathrm{au}^{-3}$, $a = -0.307\ \mathrm{au}^3\,\mathrm{mm\,s}^{-1}$, $b = +4.05\ \mathrm{mm\,s}^{-1}$).

Heisenberg exchange coupling constants J were obtained from the adiabatic energy differences of the high-spin state and broken symmetry state [Eq. (7)],[50] in which the spin-Hamiltonian $H = -2J\vec{S}_{\mathrm{Fe}}\cdot\vec{S}_{\mathrm{rad}}$ was employed.

$$J = -\frac{E_{\mathrm{hs}} - E_{\mathrm{bs}}}{\langle S^2\rangle_{\mathrm{hs}} - \langle S^2\rangle_{\mathrm{bs}}} \tag{7}$$

Acknowledgement

This work was supported by the German-Israeli Project Coordination (DIP-F6.2 to Z.G. and W.T.). S.Y. and F.N. gratefully acknowledge a grant from the German Science Foundation (NE 690/7-1) and additional financial support from the University of Bonn. We also thank Mr. Jens Mekelburger and Dr. Frank Wennmohs for technical assistance.

[1] a) J. T. Groves, *J. Inorg. Biochem.* **2006**, *100*, 434–447; b) A. Bassan, M. R. A. Blomberg, T. Borowski, P. E. M. Siegbahn, *J. Inorg. Biochem.* **2006**, *100*, 727–743; c) S. G. Sligar, T. M. Makris, I. G. Denisov, *Biochem. Biophys. Res. Commun.* **2005**, *338*, 346–354; d) S. Shaik, S. P. de Visser, F. Ogliaro, H. Schwarz, D. Schröder, *Curr. Opin. Chem. Biol.* **2002**, *6*, 556–567; e) C. E. Schulz, R. Rutter, J. T. Sage, P. G. Debrunner, L. P. Hager, *Biochemistry* **1984**, *23*, 4743–4754; f) R. Rutter, L. P. Hager, H. Dhonau, M. Hendrich, M. Valentine, P. Debrunner, *Biochemistry* **1984**, *23*, 6809–6816.

[2] a) C. E. Schulz, H. S. Song, A. Mislankar, R. D. Orosz, C. A. Reed, P. G. Debrunner, W. R. Scheidt, *Inorg. Chem.* **1997**, *36*, 406–412; b) K. Ayougou, D. Mandon, J. Fischer, R. Weiss, M. Müther, V. Schünemann, A. X. Trautwein, E. Bill, J. Terner, K. Jayaraj, A. Gold, R. N. Austin, *Chem. Eur. J.* **1996**, *2*, 1159–1163; c) H. Fujii, T. Yoshimura, H. Kamada, *Inorg. Chem.* **1996**, *35*, 2373–2377; d) K. Jayaraj, J. Terner, A. Gold, D. A. Roberts, R. N. Austin, D. Mandon, R. Weiss, E. Bill, M. Müther, A. X. Trautwein, *Inorg. Chem.* **1996**, *35*, 1632–1640; e) M. Müther, E. Bill, A. X. Trautwein, D. Mandon, R. Weiss, A. Gold, K. Jayaraj, R. N. Austin, *Hyperfine Interact.* **1994**, *91*, 803–808; f) S. Nakashima, H. Ohyanishiguchi, N. Hirota, H. Fujii, I. Morishima, *Inorg. Chem.* **1990**, *29*, 5207–5211; g) K. Jayaraj, A. Gold, R. N. Austin, D. Mandon, R. Weiss, J. Terner, E. Bill, M. Müther, A. X. Trautwein, *J. Am. Chem. Soc.* **1995**, *117*, 9079–9080; h) K. Jayaraj, A. Gold, R. N. Austin, L. M. Ball, J. Terner, D. Mandon, R. Weiss, J. Fischer, A. DeCian, E. Bill, M. Müther, V. Schünemann, A. X. Trautwein, *Inorg. Chem.* **1997**, *36*, 4555–4566; i) E. Bill, V. Schünemann, A. X. Trautwein, R. Weiss, J. Fischer, A. Tabard, R. Guilard, *Inorg. Chim. Acta* **2002**, *339*, 420–426; j) D. Mandon, R. Weiss, K. Jayaraj, A. Gold, J. Terner, E. Bill, A. X. Trautwein, *Inorg. Chem.* **1992**, *31*, 4404–4409.

[3] J. T. Groves, Z. Gross, M. K. Stern, *Inorg. Chem.* **1994**, *33*, 5065–5072.

[4] S. Shaik, D. Kumar, S. P. de Visser, A. Altun, W. Thiel, *Chem. Rev.* **2005**, *105*, 2279–3935.

[5] K. Czarnecki, S. Nimri, Z. Gross, L. M. Proniewicz, J. R. Kincaid, *J. Am. Chem. Soc.* **1996**, *118*, 2929–2935.

[6] C. E. Schulz, P. W. Devaney, H. Winkler, P. G. Debrunner, N. Doan, R. Chiang, R. Rutter, L. P. Hager, *FEBS Lett.* **1979**, *103* 102–105.

[7] a) K. L. Stone, L. M. Hoffart, R. K. Behan, C. Krebs, M. T. Green, *J. Am. Chem. Soc.* **2006**, *128*, 6147–6153; b) M. T. Green, J. H. Dawson, H. B. Gray, *Science* **2004**, *304*, 1653–1656.

[8] a) *Expanded, Contracted & Isomeric Porphyrins* (Eds.: J. L. Sessler, S. J. Weghorn), Pergamon, Oxford, **1997**; b) C. Erben, S. Will, K. M. Kadish, in *The Porphyrin Handbook, Vol. II* (Eds.: K. M. Kadish, K. M. Smith, R. Guilard), Academic Press, New York, **2000**, pp. 233–300; c) A. Aviv, Z. Gross, *Chem. Commun.* **2007**, 1987–1999; d) D. P. Goldberg, *Acc. Chem. Res.* **2007**, *40*, 626–634.

[9] a) S. Will, A. Rahbar, H. Schmickler, J. Lex, E. Vogel, *Angew. Chem.* **1990**, *102*, 1434–1437; *Angew. Chem. Int. Ed. Engl.* **1990**, *29*, 1390–1393; b) E. Vogel, *Pure Appl. Chem.* **1993**, *65*, 143–152; c) C. V. Asokan, S. Smeets, W. Dehaen, *Tetrahedron Lett.* **2001**, *42*, 4483–4485; d) R. P. Brinas, C. Brückner, *Synlett* **2001**, 442–444; e) W. S. Cho, C. H. Lee, *Tetrahedron Lett.* **2000**, *41*, 697–701; f) Z. Gross, N. Galili, I. Saltsman, *Angew. Chem.* **1999**, *111*, 1530–1533; *Angew. Chem. Int. Ed.* **1999**, *38*, 1427–1429; g) Z. Gross, N. Galili, L. Simkhovich, I. Saltsman, M. Botoshansky, D. Blaser, R. Boese, I. Goldberg, *Org. Lett.* **1999**, *1*, 599–602; h) D. T. Gryko, *Chem. Commun.* **2000**, 2243–2244; i) D. T. Gryko, K. Jadach, *J. Org. Chem.* **2001**, *66*, 4267–4275; j) J. W. Ka, W. S. Cho, C. H. Lee, *Tetrahedron Lett.* **2000**, *41*, 8121–8125; k) R. Paolesse, L. Jaquinod, D. J. Nurco, S. Mini, F. Sagone, T. Boschi, K. M. Smith, *Chem. Commun.* **1999**, 1307–1308; l) R. Paolesse, S. Nardis, F. Sagone, R. G. Khoury, *J. Org. Chem.* **2001**, *66*, 550–556; m) L. Simkhovich, I. Goldberg, Z. Gross, *J. Inorg. Biochem.* **2000**, *80*, 235–238.

[10] a) G. Golubkov, J. Bendix, H. B. Gray, A. Mahammed, I. Goldberg, A. J. DiBilio, Z. Gross, *Angew. Chem.* **2001**, *113*, 2190–2192; *Angew. Chem. Int. Ed.* **2001**, *40*, 2132–2134; b) Z. Gross, G. Golubkov, L. Simkhovich, *Angew. Chem.* **2000**, *112*, 4211–4213; *Angew. Chem. Int. Ed.* **2000**, *39*, 4045–4047; c) Z. Gross, L. Simkhovich, N. Galili, *Chem. Commun.* **1999**, 599–600; d) L. Simkhovich, A. Mahammed, I. Goldberg, Z. Gross, *Chem. Eur. J.* **2001**, *7*, 1041–1055; e) Z. Gross, H. B. Gray, *Adv. Synth. Catal.* **2004**, *346*, 165–170; f) A. Mahammed, Z. Gross, *J. Am. Chem. Soc.* **2005**, *127*, 2883–2887; g) I. Aviv, Z. Gross, *Synlett* **2006**, 951–953; h) I. Aviv, Z. Gross, *Chem. Eur. J.* **2008**, *14*, 3995–4005.

[11] a) J. Bendix, I. J. Dmochowski, H. B. Gray, A. Mahammed, L. Simkhovich, Z. Gross, *Angew. Chem.* **2000**, *112*, 4214–4217; *Angew. Chem. Int. Ed.* **2000**, *39*, 4048–4051; b) A. Mahammed, Z. Gross, *J. Inorg. Biochem.* **2002**, *88*, 305–309; c) E. Stavitski, A. Berg, T. Ganguly, A. Mahammed, Z. Gross, H. Levanon, *J. Am. Chem. Soc.* **2004**, *126*, 6886–6890; d) L. Wagnert, A. Berg, E. Stavitski, T. Berthold, G. Kothe, I. Goldberg, A. Mahammed, L. Simkhovich, Z. Gross, H. Levanon, *Appl. Magn. Reson.* **2006**, *30*, 591–604; e) L. Wagnert, A. Berg, E. Stavitski, I. Luobeznova, Z. Gross, H. Levanon, *J. Porphyrins Phthalocyanines* **2007**, *11*, 645–651.

[12] a) D. Aviezer, S. Cotton, M. David, A. Segev, N. Khaselev, N. Galili, Z. Gross, A. Yayon, *Cancer Res.* **2000**, *60*, 2973–2980; b) H. Agadjanian, J. J. Weaver, A. Mahammed, A. Rentsendorj, S. Bass, J. Kim, I. J. Dmochowski, R. Margalit, H. B. Gray, Z. Gross, L. K. Medina-Kauwe, *Pharm. Res.* **2006**, *23*, 367–377; c) A. Mahammed, Z. Gross, *Angew. Chem.* **2006**, *118*, 6694–6697; *Angew. Chem. Int. Ed.* **2006**, *45*, 6544–6547; d) Z. Gershman, I. Goldberg, Z. Gross, *Angew. Chem.* **2007**, *119*, 4398–4402; *Angew. Chem. Int. Ed.* **2007**, *46*, 4320–4324; e) A. Haber, H. Agadjanian, L. K. Medina-Kauwe, Z. Gross, *J. Inorg. Biochem.* **2008**, *102*, 446–457.

[13] L. Simkhovich, Z. Gross, *Tetrahedron Lett.* **2001**, *42*, 8089–8092.

[14] Z. Gross, *J. Biol. Inorg. Chem.* **2001**, *6*, 733–738.

[15] Z. Gross, H. B. Gray, *Comm. Inorg. Chem.* **2006**, *27*, 61–72.

[16] E. Vogel, S. Will, A. S. Tilling, L. Neumann, J. Lex, E. Bill, A. X. Trautwein, K. Wieghardt, *Angew. Chem.* **1994**, *106*, 771–775; *Angew. Chem. Int. Ed. Engl.* **1994**, *33*, 731–735.

[17] a) S. Cai, F. A. Walker, S. Licoccia, *Inorg. Chem.* **2000**, *39*, 3466–3478; b) L. Yatsunyk, F. A. Walker, *Inorg. Chim. Acta* **2002**, *337*, 266–274; c) S. Cai, S. D'Ottavi, C. Licoccia, R. Paolesse, S. Nardis, V. Bulach, B. Zimmer, T. Kh. Shokhireva, F. A. Walker, *Inorg. Chim. Acta* **2002**, *339*, 171–178; d) O. Zakharieva, V. Schünemann, M. Gerdan, S. Licoccia, S. Cai, F. A. Walker, A. X. Trautwein, *J. Am. Chem. Soc.* **2002**, *124*, 6636–6648; e) F. A. Walker, *Inorg. Chem.* **2003**, *42*, 4526–4544; f) S. Nardis, R. Paolesse, S. Licoccia, F. R. Fronczek, M. G. H. Vicente, T. K. Shokhireva, S. Cai, F. A. Walker, *Inorg. Chem.* **2005**, *44*, 7030–7046; g) F. A. Walker, S. Licoccia, R. Paolesse, *J. Inorg. Biochem.* **2006**, *100*, 810–837.

[18] L. Simkhovich, N. Galili, I. Saltsman, I. Goldberg, Z. Gross, *Inorg. Chem.* **2000**, *39*, 2704–2705.
[19] A. Ghosh, E. Steene, *J. Biol. Inorg. Chem.* **2001**, *6*, 739–742.
[20] a) E. Steene, T. Wondimagegn, A. Ghosh, *J. Phys. Chem. B* **2001**, *105*, 11406–11413; b) A. Ghosh, E. Steene, *J. Inorg. Biochem.* **2002**, *91*, 423–436.
[21] L. Simkhovich, I. Goldberg, Z. Gross, *Inorg. Chem.* **2002**, *41*, 5433–5439.
[22] a) K. M. Kadish, *Prog. Inorg. Chem.* **1986**, *34*, 435–605; b) K. M. Kadish, B. Boisselier-Cocolios, A. Coutsolelos, P. Mitaine, R. Guilard, *Inorg. Chem.* **1985**, *24*, 4521–4528.
[23] P. Gans, G. Buisson, E. Duee, J. C. Marchon, B. S. Erler, W. F. Scholz, C. A. Reed, *J. Am. Chem. Soc.* **1986**, *108*, 1223–1234.
[24] A. Bencini, D. Gatteschi, *EPR of Exchange Coupled Systems*, Springer, Berlin, **1990**.
[25] G. P. Gupta, G. Lang, C. A. Reed, K. Shelly, W. R. Scheidt, *J. Chem. Phys.* **1987**, *86*, 5288–5293. The porphyrin complex [Fe^{III}(tpp)-($FSbF_5$)] discussed in this paper is described as spin admixed species with 98% $S=3/2$ character in the ground state. We must refrain from a detailed comparison of zero-field splitting and hyperfine parameters, because the magnetic susceptibility and Mössbauer data are not parameterized by using the usual spin Hamiltonian model for $S=3/2$, but with an extended model with parameters that can, unfortunately, not directly be compared with the D and A parameters used here.
[26] K. L. Kostka, B. G. Fox, M. P. Hendrich, T. J. Collins, C. E. F. Rickard, L. J. Wright, E. Münck, *J. Am. Chem. Soc.* **1993**, *115*, 6746–6757.
[27] H. Keutel, I. Käpplinger, E.-G. Jäger, M. Grodzicki, V. Schünemann, A. X. Trautwein, *Inorg. Chem.* **1999**, *38*, 2320–2327.
[28] K. Chłopek, E. Bill, T. Weyhermüller, K. Wieghardt, *Inorg. Chem.* **2005**, *44*, 7087–7098.
[29] a) J. C. Schöneboom, F. Neese, W. Thiel, *J. Am. Chem. Soc.* **2005**, *127*, 5840–5853; b) M. R. Bukowski, K. D. Koehntop, A. Stubna, E. L. Bominaar, J. A. Halfen, E. Münck, W. Nam, *Science* **2005**, *310*, 1000–1002; c) A. Atanasov, P. Comba, C. A. Daul, F. Neese in *Models, Mysteries and Magic of Molecules* (Eds.: J. Boeyens, J. Ogilvie), Springer, Berlin, **2008**; d) W. T. Oosterhuis, G. Lang, *J. Chem. Phys.* **1973**, *58*, 4757–4765; e) H. Paulsen, M. Müther, M. Grodzicki, A. X. Trautwein, E. Bill, *Bull. Soc. Chim. Fr.* **1996**, *133*, 703–710.
[30] D. Niarchos, A. Kostikas, A. Simopoulos, D. Coucouvanis, D. Piltingsrud, R. E. Coffman, *J. Chem. Phys.* **1978**, *69*, 4411–4418.
[31] K. L. Kostka, B. G. Fox, M. P. Hendrich, T. J. Collins, C. E. F. Rickard, L. J. Wright, E. Münck, *J. Am. Chem. Soc.* **1993**, *115*, 6746–6757.
[32] P. Ghosh, E. Bill, T. Weyhermüller, K. Wieghardt, *J. Am. Chem. Soc.* **2003**, *125*, 3967–3979.
[33] K. Chłopek, E. Bill, T. Weyhermüller, K. Wieghardt, *Inorg. Chem.* **2005**, *44*, 7087–7098.
[34] F. Neese, *Inorg. Chim. Acta* **2002**, *337*, 181–192
[35] N. Godbout, R. Havlin, R. Salzmann, P. G. Debrunner, E. Oldfield, *J. Phys. Chem. A* **1998**, *102*, 2342–2350.
[36] S. Sinnecker, N. Svensen, E. W. Barr, S. Ye, Jr., J. M. Bollinger, Jr., F. Neese, C. Krebs, *J. Am. Chem. Soc.* **2007**, *129*, 6168–6179.
[37] F. Neese, *J. Phys. Chem. Solids* **2004**, *65*, 781–785.
[38] E. Steene, A. Dey, A. Ghosh, *J. Am. Chem. Soc.* **2003**, *125*, 16300–16309.
[39] F. Neese, ORCA—An ab initio, Density Functional and Semiempirical Program Package Version 2.5–20.2007 ed., Universität Bonn, Bonn (Germany), **2007**.
[40] a) A. D. Becke, *Phys. Rev. A* **1988**, *38*, 3098–3100; b) J. P. Perdew, *Phys. Rev. B* **1986**, *34*, 7406; c) J. P. Perdew, *Phys. Rev. B* **1986**, *33*, 8822–8824.
[41] a) A. D. Becke, *J. Chem. Phys.* **1993**, *98*, 5648–5652; b) C. T. Lee, W. T. Yang, R. G. Parr, *Phys. Rev. B* **1988**, *37*, 785–789.
[42] a) A. Schäfer, C. Huber, R. Ahlrichs, R. *J. Chem. Phys.* **1994**, *100*, 5829–5835; b) The basis sets can be downloaded from the ftp server of the Turbomole home page: http://www.turbomole.com.
[43] A. Schäfer, C. Huber, R. Ahlrichs, *J. Chem. Phys.* **1994**, *100*, 5829–5835.
[44] a) K. Eichkorn, F. Weigend, O. Treutler, R. Ahlrichs, *Theor. Chem. Acc.* **1997**, *97*, 119–124. b) K. Eichkorn, O. Treutler, H. Öhm, M. Häser, R. Ahlrichs, *Chem. Phys. Lett.* **1995**, *240*, 283–290.
[45] K. Eichkorn, O. Treutler, H. Öhm, M. Häser, R. Ahlrichs, *Chem. Phys. Lett.* **1995**, *242*, 652–660.
[46] F. Neese, G. Olbrich, *Chem. Phys. Lett.* **2002**, *362*, 170–178.
[47] a) B. Kirchner, F. Wennmohs, S. Ye, F. Neese, *Curr. Opin. Chem. Biol.* **2007**, *11*, 134–141. b) S. C. Bart, K. Chłopek, E. Bill, M. W. Bouwkamp, E. Lobkovsky, F. Neese, K. Wieghardt, P. J. Chirik, *J. Am. Chem. Soc.* **2006**, *128*, 13901–13912.
[48] S. Sinnecker, L. P. Slep, E. Bill, F. Neese, *Inorg. Chem.* **2005**, *44*, 2245–2254.
[49] D. A. Pantazis, X.-Y. Chen, C. R. Landis, F. Neese, *J. Chem. Theory Comput.* **2008**, *4*, 908–919.
[50] a) K. Yamaguchi, Y. Takahara, T. Fueono in *Applied Quantum Chemistry* (Eds.: V. H. Smith), Reidel, Dordrecht, **1986**, p. 155; b) T. Soda, Y. Kitagawa, T. Onishi, Y. Takano, Y. Shigeta, H. Nagao, Y. Yoshioka, K. Yamaguchi, *Chem. Phys. Lett.* **2000**, *319*, 223–230.

Received: June 25, 2008
Published online: October 27, 2008

